Reverse Undercompressive Shock Structures in Driven Thin Film Flow

Jeanman Sur*, Andrea L. Bertozzi**,*, and Robert P. Behringer*
*Department of Physics and Center for Nonlinear and Complex Systems,
**Department of Mathematics,
Duke University, Durham, NC 27708
(January 10, 2003)

We show experimental and computational evidence of a new structure: an undercompressive and reverse undercompressive shock for draining films driven by a surface tension gradient against gravity. The reverse undercompressive shock is unstable to transverse perturbations while the leading undercompressive shock is stable. Depending on the pinch-off film thickness, as controlled by the meniscus, either a trailing rarefaction wave or a compressive shock separates from the reverse undercompressive shock.

PACS numbers: 68.15.+e,68.45.Gd,03.40.Gc,47.20.Ma

Thin coating flows, as reviewed recently [1], are of great technical and scientific interest. Practical examples include spin coating, thin films coating the lungs, paints, and microfluidic devices. Scientifically, the advancing front of a driven film is an important example of shock formation in a system described by a scalar conservation law. Until recently, it was believed that for such systems, only compressive shocks could occur in which characteristics enter the shock from each side. Experiments on thermally driven films by Cazabat et al. [2,3] showed, for the first time, that novel undercompressive (UC) shocks occur in thin films, for which characteristics enter the shock on one side and leave on the other. This work has stimulated new theory for these problems [4,5]. Here, we show new experimental evidence of a completely different type of undercompressive shock in such a system. This "reverse undercompressive shock" (RUC) involves a thicker film receding from a thinning region. Unlike the wave found in [2], the RUC shock is unstable to transverse perturbations.

The basic experiment consists of a thin film on an inclined substrate that is driven against gravity by a surface tension (γ) gradient. The gradient in γ is due to a temperture gradient (Marangoni effect) as in the work of Cazabat et al. (Cal) [6,7]. As the film advances, a capillary ridge forms which in turn can lead to a fingering instability similar to that in gravitationally driven films [8] if α, the inclination angle from horizontal, is large enough [2,3,9]. This transition reflects a basic change in the dynamics of the film: very thin film fronts (larger α) show a single shock profile that is unstable to fingering [10]; thicker films exhibit an undercompressive-compressive shock pair [2,5] in which the leading UC front is stable [4,10].

In this Letter we present experimental and numerical evidence of a new structure involving a pair of UC shocks for a film that is both draining into a reservoir under gravity, and advancing up a substrate due to a gradient in γ (Fig. 1) as in the older work by Ludviksson and Lightfoot [11] (LL). The double shock structure for this situation was recently proposed by Münch [12]. He predicts that the meniscus region pinches off a body of fluid that travels up the substrate almost as a solitary wave, where both the leading and trailing fronts are undercompressive. The trailing undercompressive front has never been documented in experiments, although its existence follows rigorously from the analysis of [13]. Münch calls this trailing front a 'reverse undercompressive' (RUC) shock because it involves a thicker film advancing upward from a thinner film, which is the reverse of the type found by Cazabat et al. [2,3], where a UC shock describes a thicker film advancing into a thinner region.

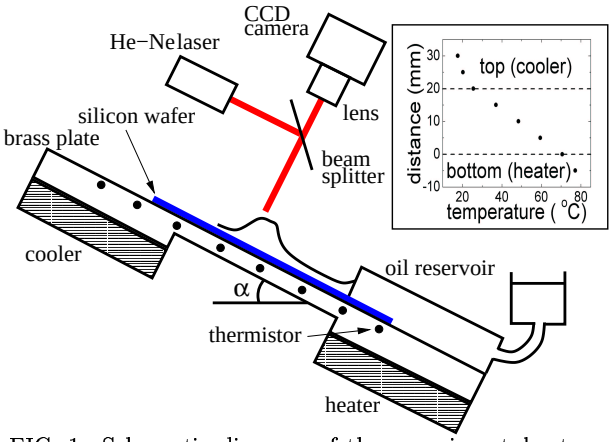

FIG. 1. Schematic diagram of the experimental setup. A typical temperature gradient is shown in the inset.

The experiments are carried out as follows. An oxidized silicon wafer is partially dipped into a reservoir of silicone oil (PDMS, η=100 cSt and γ=0.0209 N/m at 25^{o}C) and attached to a brass plate. The wafer is pulled out and clamped to the plate (Fig. 1). We create a uniform temperature gradient along the plate by heating at the bottom with a foil heater and cooling at the top with a circulating bath cooler. We monitor the temperature along the plate via thermistors. A typical gradient, which is constant during an experiment, is shown in the inset

of Fig. 1. The distance between the heater and cooler is 20 mm, and the width of the brass plate is 152 mm (effectively infinite width in the transverse direction).

We measure the thickness of the film by both standard interferometric techniques and by a novel variation of this technique. The primary technique uses collimated light from a He-Ne laser (wavelength 632.8 nm) incident normally on the film. We record images with a CCD camera and a frame grabber. Additionally, at the end of a run, we shine an infrared laser (830 nm, 100 mW) at a point on the film. The film near the laser spot is reduced to essentially zero thickness due to the combination of local heating and the induced surface tension gradient. We then measure the thickness at other points on the film by counting the interference fringes from the reference position (One fringe = $0.226\mu m$.) We have less precision determining the absolute thickness of very thick regions, although the relative error between nearby fringes is small. This is reflected in the larger absolute error bar shown in the top right corner of Figs. 5 and 6.

In addition to experiments, we model the dynamics of the draining film using the lubrication approximation with a 'depth averaged' velocity [2]

$$\vec{V} = (\frac{\tau h}{2\eta} - \frac{\rho g h^2 \sin\alpha}{3\eta})\vec{e}_x + \frac{\gamma h^2 \nabla^3 h}{3\eta}. \qquad (1)$$

We model the meniscus as a boundary condition that we discuss later. In the above, h denotes film thickness, $\tau = d\gamma/dx$ the surface tension gradient, α the angle of inclination (from the horizontal) of the plane, g the gravitational constant, ρ density of the fluid. Also, x is along the direction of the flow. The coefficient of $\vec{e}_x$ in Eq. (1) represents convection due to the surface tension gradient and the component of gravity tangent to the surface. The component of gravity normal to the surface has a negligible effect. We couple Eq. (1) with mass conservation, $h_t + \nabla \cdot (h\vec{V}) = 0$. To understand the shock dynamics, we ignore perturbations transverse to $\vec{e}_x$ and consider solutions h depending only on x and t: $h_t + (f(h))_x = -((\gamma/3\eta)h^3 h_{xxx})_x$. The flux satisfies $f(h) = (\tau h^2/2 - \sin\alpha\rho g h^3/3)/\eta$. We rescale to dimensionless units as in [2]: $h = H\hat{h}$, $x = \hat{x}l$, and $t = T\hat{t}$, where $H = \frac{3\tau}{2\sin\alpha\rho g}$, $l = (\frac{2\gamma}{3\tau H^2})^{1/3} = (\frac{3\gamma\tau}{2\rho^2 g^2 sin^2\alpha})^{1/3}$, and $T = 2\frac{\eta}{\tau^2}(\frac{4}{9}\tau\gamma\rho g sin\alpha)^{1/3}$. Dropping the $\hat{}$ gives the dimensionless equation

$$h_t + (h^2 - h^3)_x = -(h^3 h_{xxx})_x. \qquad (2)$$

We now turn to a description of the experimental results. In the early stage of the film evolution, a stationary pinched-off portion appears in the meniscus, as predicted by Münch [12], while the contact line climbs. Later, a RUC shock moves up from the pinched-off portion and a broadening rarefaction wave (RW) appears between the meniscus and the RUC shock as in Fig. 2.

In the experiments, the leading UC shock is stable, while the RUC shock becomes unstable and begins to finger as predicted [12]. The dimensionless fingering wavenumber ($2\pi l/\lambda$, λ = wavelength) of the RUC shock is $0.39 \pm .02$ which is measured from Figs. 2(a) and 3(a) and is close to the most unstable wavenumber of 0.35 predicted by linear theory [12]. As the film evolves, a flat region ($h_{\rm RUC}$) appears just behind the RUC shock.

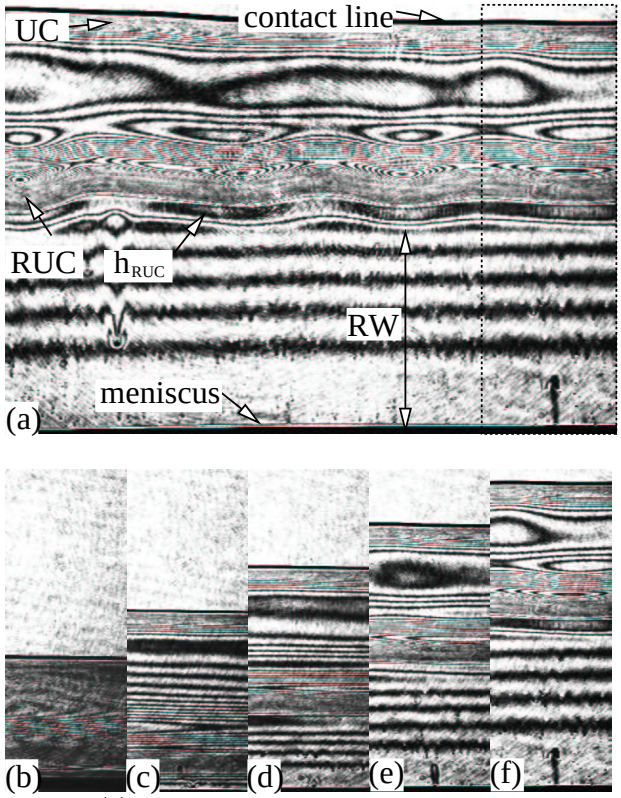

FIG. 2. (a) Interference fringes at t = 3200 sec. for $\alpha = 85°$ and $\tau = 0.11$ Pa. The vertical and the horizontal size are 14.4 mm and 19.2 mm respectively. Below are sections (as indicated by the dashed line in (a)) at times (b) 0 sec, (c) 800 sec, (d) 1600 sec, (e) 2400 sec, and (f) 3200 sec.

The film thickness $h_{\rm eq}$ just above the meniscus is determined by balancing surface tension gradient, gravity, and curvature [7]. Thus, the inclination angle and the surface tension gradient control $h_{\rm eq}$. Here, we fix $d\gamma/dx$ and we vary α to control $h_{\rm eq}$. Decreasing α, leads to increasing $h_{\rm eq}$ and $h_{\rm eq} - h_{\rm RUC}$. If $h_{\rm eq} > h_{\rm RUC}$, then a flat region with a compressive shock (CS) replaces the rarefaction wave just behind the $h_{\rm RUC}$ region as in Fig. 3.

The position of the leading UC shock is linear in time, while the RUC shock shows transient nonlinear motion, consistent with the theoretical model (see below). The leading UC shock is the same as the one observed in the Cal experiments and the speed is the same as in [3]. The RUC shock is always faster than the leading UC shock, so that the size of the bump diminishes. The RUC shock position as a function of time for different inclination angles all collapse to a common curve when the position is rescaled by l, and time is rescaled by T, as shown in Fig. 4.

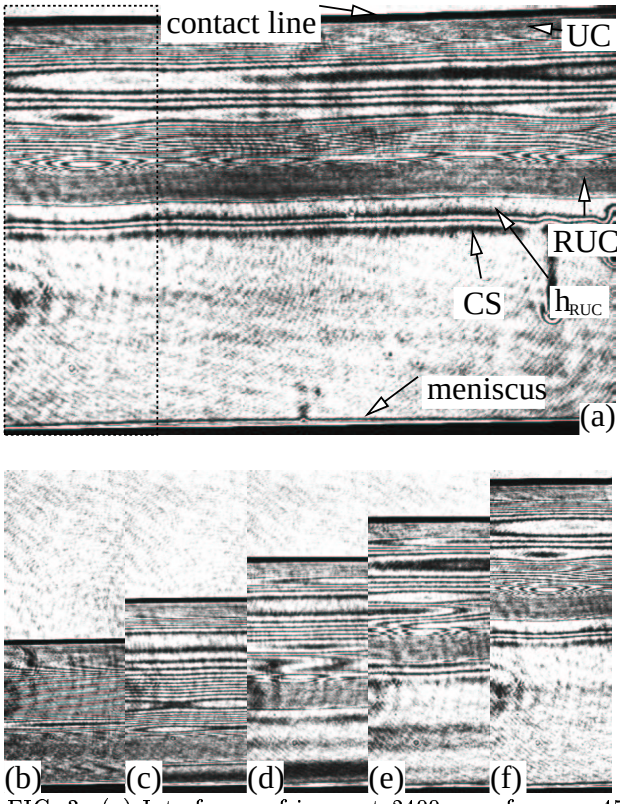

FIG. 3. (a) Interference fringes at 2400 sec. for $\alpha = 45°$ and $\tau = 0.11$ Pa. The dimensions are as in Fig. 2. Sections (dashed region) are shown at (b) 0 sec, (c) 600 sec, (d) 1200 sec, (e) 1800 sec, and (f) 2400 sec.

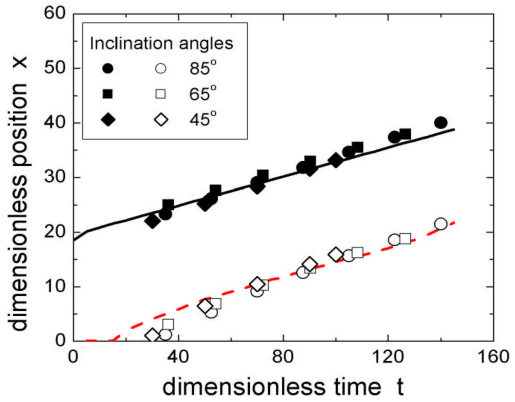

FIG. 4. The position of the contact line (solid symbols) and the position of the reverse undercompressive shock (open symbols) versus time. Theory, as predicted from the computation from Fig. 5 shown as solid and dashed lines.

To compare the experimental data with the model, we need boundary and initial conditions. Ahead of the contact line, we choose the simplest boundary condition consistent with complete wetting: a precursor model with $h \to b > 0$ as $x \to \infty$ [2,14,15]. As shown previously [2,3,16], b determines both the height and speed of the leading UC shock. This in turn determines the height and speed of the trailing reverse undercompressive wave. We find that $b = 0.005$ gives the best approximation of the leading edge of the advancing film in these experiments. In the model, we take $x = 0$ to be the position of the edge of the meniscus. For the lower boundary condition, we assume the meniscus has just pinched off a film of thickness $h = h_{\rm eq}$ with zero third derivative $h_{xxx}(0) = 0$, i.e. that the meniscus enforces a zero net curvature gradient on the bulk film region. This initial condition is the simplest approximation of a draining film, that of constant film thickness h_f for the range $0 < x < x_f$. The parameter x_f is determined from the experiments by measuring the distance between the meniscus and the contact line at t = 0 in Figs. 2(b) and 3(b). We also measure the height and width of the bump at a late stage to determine the cross sectional volume V_f (= width × height) which is used to determine the initial height h_f ($= V_f/x_f$). Actually, the width of the bump decreases with time because the mass in the bump drains into the flat region $h_{\rm RUC}$. However, the volume of the bump remains nearly constant because the width of $h_{\rm RUC}$ is much smaller than that of the bump.

We numerically integrate (2) forward in time with initial and boundary conditions and compare with the experimental data in Figs. 2 and 3. The viscosity varies with temperature in the experiment. We choose a viscosity for the time rescaling of (2) that is optimized for agreement with the data while consistent with the experiment.

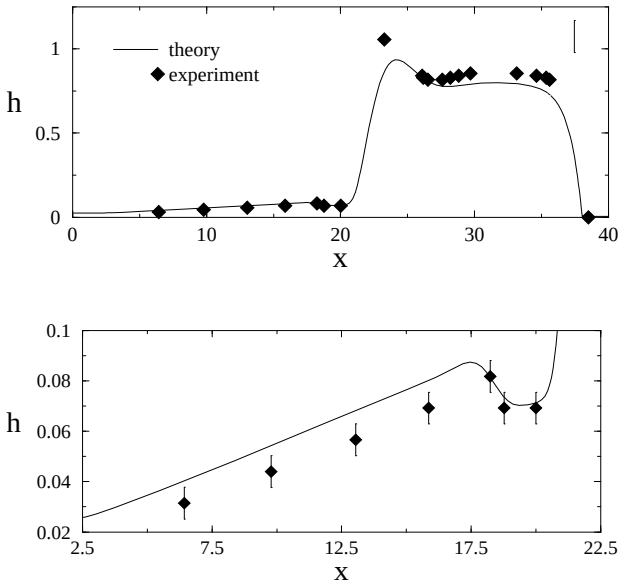

FIG. 5. Comparison between PDE theory and experiment for data from Fig. 2a. Numerical parameters are $h_{\rm eq} = 0.025$ ($0.45\mu m$), $h_f = 0.75$ ($13.6\mu m$), $x_f = 18$ ($6.2mm$). The bottom figure shows a close up of the rarefaction wave. The bar in the top right corner is the absolute error for $h > 0.5$. The absolute error for smaller h is shown on the bottom figure. The relative error for $h > 0.5$ equals the absolute error for the small h values.

Fig. 5 shows the theoretical thickness profile compared with the experiment from Fig. 2a, the dimensionless time is 140. The numerical solution evolves into a structure composed of a leading UC shock, trailing RUC shock, and expanding rarefaction wave, shown closeup in the bottom portion of Fig. 5. The leading UC shock speed and height are determined by the precursor thickness as in previous studies [2,3]. The RUC shock speed and height are determined by the height of the leading UC shock, and hence also determined by the precursor. Fig. 5 shows a well developed structure. However at early times the RUC experiences a period of adjustment before it settles into a traveling wave shape, while the leading UC shock forms almost immediately. The trailing rarefaction wave expands between the meniscus region (set by the boundary condition $h_{\rm eq}$ in the model) and the RUC shock. The trailing side of the RUC shock has a thickness $h_{\rm RUC}$. If $h_{\rm RUC}$ is greater than $h_{\rm eq}$, a rarefaction wave forms between the RUC shock and the meniscus. Otherwise a compressive shock forms to connect the meniscus pinch-off thickness $h_{\rm eq}$ to the thickness $h_{\rm RUC}$. This compressive shock is seen to slowly separate from the RUC shock. Fig. 6, compares the PDE solution with the data from Fig. 3a, in which $h_{\rm eq} > h_{\rm RUC}$. A compressive shock forms to the left of the RUC shock, as shown close up in the bottom of Fig. 6. At this α of 45°, we are close to this transition point, and the experimental results are quite sensitive to changes in the initial draining film profile.

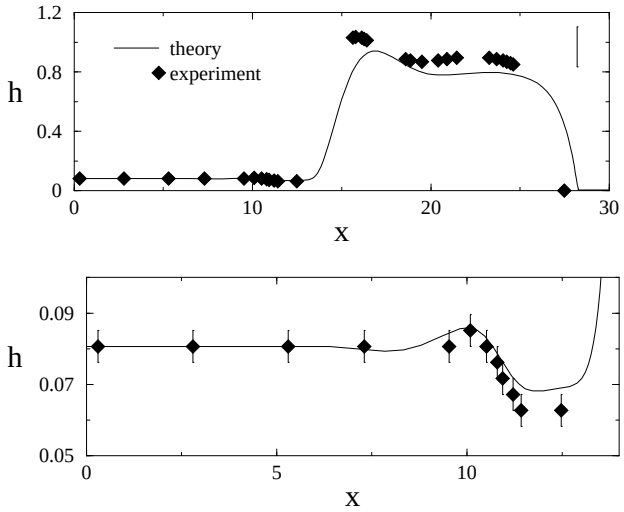

FIG. 6. Comparison between PDE theory and experiment for data from Fig. 3a, numerical parameters are $h_{\rm eq} = 0.081$ $(2.06\mu m)$, $h_f = 0.75$ $(19.1\mu m)$, $x_f = 15.4$ $(6.6mm)$. The error bars are as in Fig. 5.

The variation in viscosity (due to temperature change) along the direction of the flow is not considered in the model here but plays a modest role in the experiment. The strongest effect is on the timescale. There are weaker effects including the jump heights for the shocks. The viscosity variation across the bump in Figs. 5 and 6 is roughly 20%, which should not dramatically affect the applicability of the theory here. A worse case estimate for the change in height due to this effect is roughly 20% which is comparable to the absolute error bar in Figs. 5 and 6. A careful analysis of where the viscosity variation occurs will be presented elsewhere.

The experiments presented show clear evidence of the new UC-RUC double shock structure predicted by Münch. The experiment compares well with a lubrication model in which the pinch-off dynamics of the meniscus are incorporated into a boundary condition. The dynamics between the RUC shock and the meniscus can result in either a rarefaction wave or a compressive shock, depending on the pinch-off thickness relative to the film thickness $h_{\rm RUC}$. Both situations are seen in the experiment and compared with theory. Future studies should address the nonlinear dynamics of the trailing RUC shock.

We thank A. Münch for sharing an advanced copy of his manuscript and A. M. Cazabat for helpful comments about the experiment. This work is supported by NSF grant DMS-0074049 and ONR grant N000140110290.

[1] A. Oron, S. H. Davis, and S. G. Bankoff, Rev. Mod. Phys., **69**(3), 931 (1997), T. G. Myers, SIAM. Rev., **40** (3), 441 (1998).
[2] A. L. Bertozzi, A. Münch, X. Fanton, and A. M. Cazabat, Phys. Rev. Lett. **81**, 5169(1998).
[3] M. Schneemilch and A. M. Cazabat., Langmuir **16**, 8796(2000); **16**, 9850(2000).
[4] A. L. Bertozzi, A. Münch, M. Shearer, and K. Zumbrun, Eur. J. Appl. Math. **12**, 253(2001).
[5] A. L. Bertozzi, A. Münch, and M. Shearer, Physica D **134**, 431(1999).
[6] A. M. Cazabat, F Heslot, S. M. Troian, and P. Carles, Nature **346**, 6287(1990).
[7] P. Carles and A. M. Cazabat, J. Coll. Int. Sci. **157**, 196(1993).
[8] H. Huppert, Nature **300**, 427(1982).
[9] X. Fanton, A. M. Cazabat, and D. Quéré, Langmuir **12**, 5875(1996).
[10] D. E. Kataoka and S. M. Troian, J. Coll. Int. Sci. **192**, 350(1997); **203**, 335(1998).
[11] V. Ludviksson and E. N. Lightfoot, Am. Inst. Chem. Engrs. J. **17**, 1166(1971).
[12] A. Münch, preprint, (2002).
[13] A. L. Bertozzi and M. Shearer, SIAM J. Math. Anal. **32**, 194(2000).
[14] A. L. Bertozzi and M. P. Brenner, Phys. Fluids **9**, 530(1997).
[15] S. M. Troian, E. Herbolzheimer, S. A. Safran, and J. F. Joanny, Europhys. Lett. **10**, 25(1989).
[16] A. Münch and A. L. Bertozzi, Phys. Fluids **11**, 2812(1999).